

Identification of soft modes in amorphous Al_2O_3 via first-principles

Alexander C. Tyner^{1,2,*}, Joshua T. Heath^{1,2}, Thue Christian Thann³, Vincent P.

Michal³, Peter Krogstrup³, Mark Kamper Svendsen³, and Alexander V. Balatsky^{1,2}

¹ Nordita, KTH Royal Institute of Technology and Stockholm University 106 91 Stockholm, Sweden

² Department of Physics, University of Connecticut, Storrs, Connecticut 06269, USA and

³ NNF Quantum Computing Programme, Niels Bohr Institute, University of Copenhagen, Denmark

(Dated: February 21, 2025)

Amorphous Al_2O_3 is a fundamental component of modern superconducting qubits. While amorphous oxides offer distinct advantages, such as directional isotropy and a consistent bulk electronic gap, in realistic systems these compounds support two-level systems (TLSs) which couple to the qubit, expediting decoherence. In this work, we perform a first-principles study of amorphous Al_2O_3 and identify low-energy modes in the electronic and phonon spectra as a possible origin for TLSs.

I. INTRODUCTION

In recent years, superconducting qubits have emerged as a leading platform for quantum computation in both academia and industry [1–4]. The existence of two-level systems (TLS) within superconducting qubits have been proposed as a contributing factor to the rate of decoherence [5–15]. Despite the presence of TLSs, amorphous Al_2O_3 remains well suited for use in superconducting qubits, as the lack of long range order has the consequence of making the electronic properties directionally isotropic. Amorphous Al_2O_3 can be customized to a variety of architectures without concern for grain-boundaries and other complications of cleaving crystalline compounds[16], and is dynamically stable with robust electronic properties [17, 18].

The hypothesis we investigate is that localized low-frequency phonons in amorphous Al_2O_3 may be considered as TLSs. These “soft localized modes” oscillate with frequencies that are much lower than the typical Bose peak and Debye energies. Hence, once quantized, these modes can induce local TLS dynamics and induce decoherence at low frequencies. This hypothesis has been put forth in other studies however, to the best knowledge of the authors, an attempt to directly compute the phonon modes of amorphous Al_2O_3 via first-principles has yet to be put forth. To investigate this proposal, we generate multiple amorphous samples[19–22]. The starting point for generation of these samples is supercells of the ordered solid. The ordered solids are then melted using Car-Parinello molecular dynamics [23]. Multiple annealing cycles are then carried out until the samples exhibit stability at room temperature. Prior to computation of electronic properties and phonon modes, relaxation of the atomic positions at zero temperature is performed via density functional theory.

The low-frequency phonon modes of the resulting amorphous oxides are computed using density functional perturbation theory and mapped in real-space. Our results provide evidence that, when relaxed at zero-

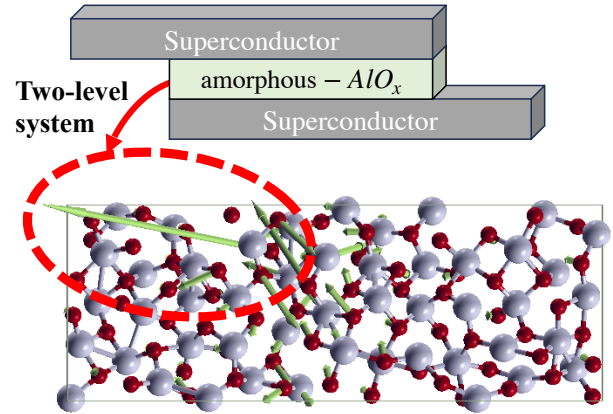


FIG. 1: Schematic of a Josephson junction for which amorphous aluminum oxide is used as the insulating barrier. We identify low-frequency modes in real space within the amorphous oxide, corresponding to two-level systems which couple to the qubit and hasten decoherence.

temperature, amorphous Al_2O_3 support phonon modes at or below 1THz localized in real-space, in alignment with the expectation for a TLS. We chose to examine the window of 0-1 THz rather than the more restricted range of 1-10 GHz at which a qubit generally operates as our first-principles computations encounter finite size effects which can harden soft modes in amorphous solids, shifting frequencies higher[24]. This is discussed as well as potential mitigation strategies through the use of alternate amorphous oxides.

II. GENERATION OF AMORPHOUS OXIDES

Unlike in the analysis of crystalline systems, structure files are not readily available for amorphous systems. This is because amorphous systems lack long range order, making each sample distinct from all others. In order to extract universal features we must follow similar procedures to those used to study disordered systems. Namely, we must use as large a system size as possible

* alexander.tyner@su.se

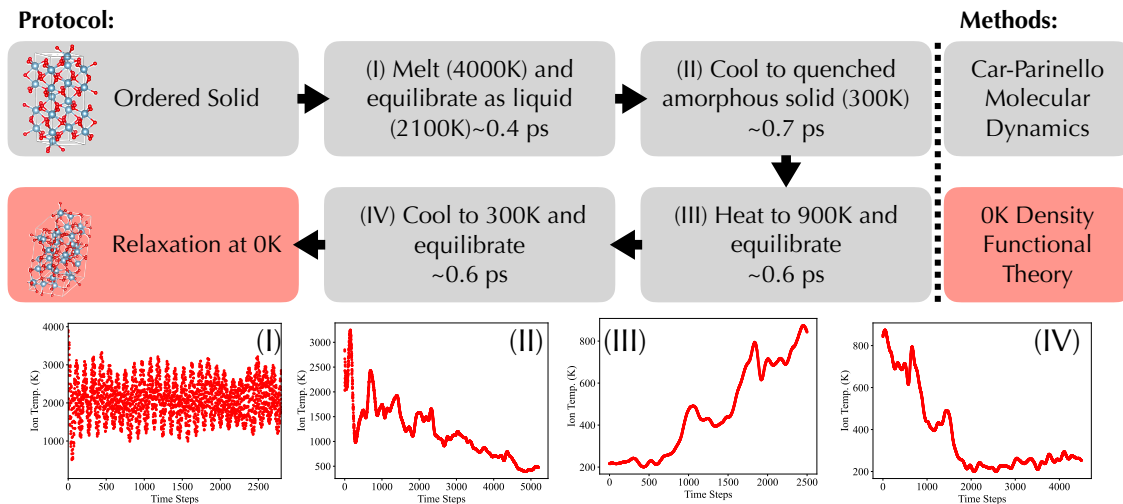


FIG. 2: Protocol for generating amorphous samples of Al_2O_3 utilizing Car-Parinello molecular dynamics. The samples are then relaxed at zero temperature using density functional theory.

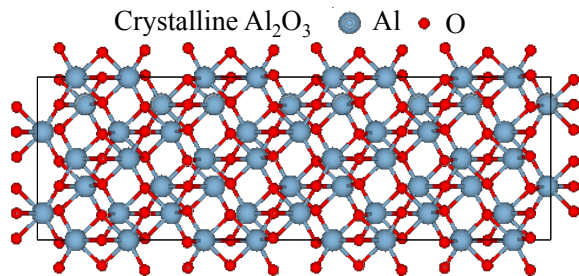


FIG. 3: A $2 \times 1 \times 2$ sample of Al_2O_3 in the ordered crystalline phase containing a total of 120 atoms. This is the starting point for the molecular dynamics protocol to generate amorphous samples.

and average over multiple distinct structures in an attempt to recover universal properties and limit finite size effects. Variations of the finite state samples reflect the variability of the amorphous Al_2O_3 structure in realistic junctions.

In order to generate the structures we begin with ordered crystals of Al_2O_3 in spacegroup $R\bar{3}c$. A supercell of 120 atoms is formed. These ordered crystals are shown in Fig. (3).

A. Generation of amorphous Al_2O_3 samples

To form the amorphous structures we follow a procedure put forth in Ref. [19] for the generation of amorphous SiO_x utilizing Car-Parinello molecular dynamics (CPMD) as implemented within the Quantum Espresso software package[25, 26]. The procedure is summarized here and shown schematically in Fig. (2). First, the atoms are randomly displaced from their starting posi-

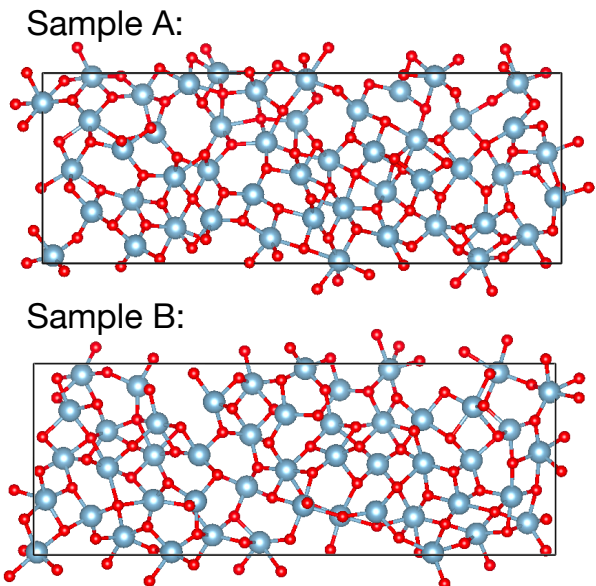


FIG. 4: Two of the generated amorphous samples of Al_2O_3 at zero temperature. Each sample is unique in accordance with the lack of order in amorphous systems.

tions, shown in Fig. (3), by a maximum of 2 percent of the lattice vector magnitude in each direction. Throughout the CPMD computations we use a $5 \times 5 \times 5$ real-space mesh for the wavefunction and charge density FFT. A plane-wave cutoff of 35 Ry, a timestep of 5.5 a.u. (1 a.u. = $2.4189 \times 10^{-17} \text{s}$), a fictitious electron mass of 300 a.u. (1 a.u. = $9.10939 \times 10^{-31} \text{kg}$)[19] and non-relativistic pseudopotentials from the pseudodojo [27] data base are used.

After the atomic positions are randomized the structures are melted by rescaling the velocities to reach a

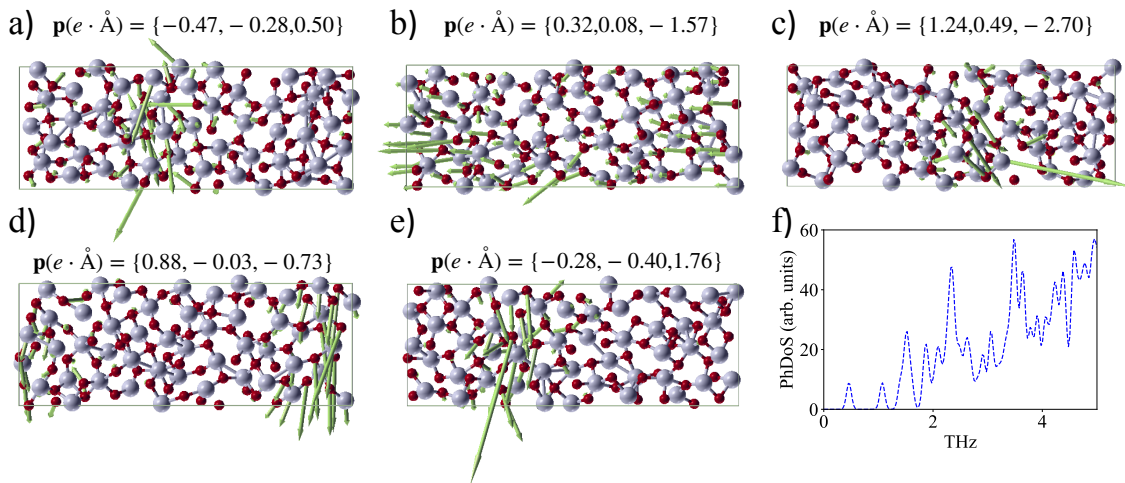


FIG. 5: (a)-(e) Displacement vectors are shown for each atom for the lowest frequency phonon modes at the Γ location for 5 distinct samples of amorphous Al_2O_3 . The dipole moment computed for each phonon mode is listed above. The phonon modes all fall within the range 0-1 THz and the modes appear localized in real-space. This observation in accordance with magnitude of the electronic dipole moments provide evidence for these phonon modes as two-level systems within a superconducting qubit. (f) Phonon density of states upon averaging over all amorphous samples.

temperature of $4000 \pm 400\text{K}$, which is above the melting point of 2345K [28], for 200 time steps. In this period the system becomes liquid-like. We then apply Nose-Hoover thermostats to the ions and electrons. The ion thermostat is set to 2100K and a characteristic frequency of 15 THz, determined by the peak in the crystalline phonon density of states. For the electrons the thermostat was set to a target kinetic energy of 0.0075 a.u. and a characteristic frequency of 1350 THz. The liquid phase is equilibrated for 2800 time steps within the canonical ensemble. We then cool this sample at a rate of $2.4 \times 10^{15} \text{K s}^{-1}$. At this rate the sample is quenched from 2100K to 300K in $\sim 0.7\text{ps}$. To ensure stability, the amorphous structure is then put through a secondary annealing cycle in which the temperature is raised to 900K over the course of 0.1ps , equilibrated at this temperature for 0.53ps and then cooled to 300K over 0.25ps . Finally, the system is allowed to equilibrate at 300K for 3500 time steps. The final structure is then allowed to evolve within an NVE ensemble and does not deviate significantly in temperature after 3500 time steps indicating stability.

Finally, the structure which is stable at 300K is the relaxed using density functional theory at zero temperature using a plane-wave cutoff of 50 Ry and a $8 \times 4 \times 2$ grid of \mathbf{k} -points. We use such a fine mesh in relaxation to increase accuracy and avoid spurious negative frequency modes in the subsequent phonon computations. The atomic positions are relaxed until the system satisfies the constraint that forces are all less than 10^{-5} Ry/Bohr ; this is referred to as the final structure. This process was used to generate five samples for which the structure files are available on GitHub. Examples of the final structures are shown in Fig. (4).

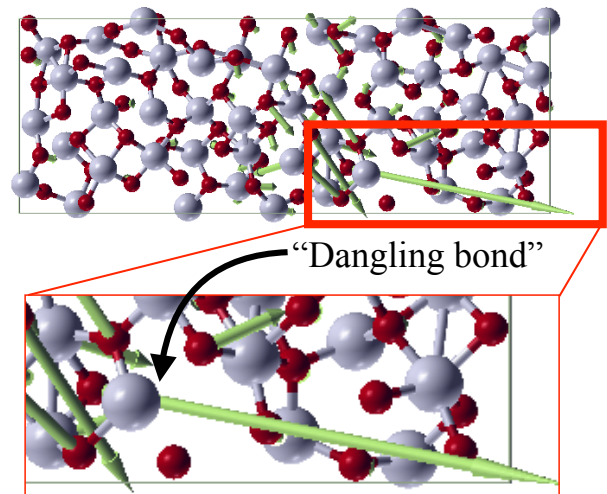


FIG. 6: Enlarging the subset of atoms with maximal displacement vectors for lowest frequency phonon mode of amorphous Al_2O_3 sample, revealing that the largest displacement vector corresponds to an Al atom which exhibits increased isolation in real-space from the sample, allowing for a dangling bond-like feature.

III. LOW-FREQUENCY PHONON MODES

We now examine the phonon modes of each sample to search for evidence to support or reject the hypothesis that low-frequency modes exist, localized in real space, which serve as TLSs coupling to the qubit. To compute the low-frequency phonon modes we utilize density functional perturbation theory (DFPT) within Quantum

Espresso. We limit our computation of phonon modes to the Γ location as the system is not an ordered solid. The lowest-energy phonon modes for each of the samples along with the phonon density of states upon averaging over each sample are shown in Fig. (5).

Examining the density of states we note that the observed, localized low-frequency modes are located primarily in the range $\approx 0.2\text{--}0.5$ THz. It is important to address that this is not the expected frequency of ~ 10 GHz expected for a TLS which couples strongly to the qubit. However, this is not entirely surprising and is likely due in part to finite size effects. Low-frequency modes are long wavelength and may be artificially hardened by size constraints and artificial periodicity invoked by density functional theory. Future work is required to accommodate > 1000 atoms, creating a unit cell sufficiently large to limit the effects of artificial periodicity. Machine learned interatomic potentials appear ideally positioned to tackle this future challenge[29–31].

As TLSs interact with qubits primarily through their electric dipole moment[32], the dipole moment of each mode is computed and displayed along with the respective phonon mode in Fig. (5). The dipole moment is computed as,

$$p_\alpha = \sum_{\kappa} Z_{\kappa,\alpha} \Delta_{\kappa,\alpha} \quad (1)$$

where $Z_{\kappa,\alpha}$ is the α component of the Born effective charge tensor for atom κ computed via DFT and $\Delta_{\kappa,\alpha}$ is similarly the displacement along α for atom κ for a given phonon mode. The expected dipole moment of a TLS in superconducting qubits has been estimated to be $\sim 0.54e\text{\AA}$ [33]. This is in excellent agreement with the dipole moment computed for each of the low-frequency modes, providing evidence towards their classification as dipole activated TLSs.

In order to qualitatively understand the origin of these low-frequency modes we can zoom in on the structure in the region for which the displacement vectors are maximal. Doing so, we observe that these large displacement vectors occur for atoms which exhibit spatial isolation to a greater extent than their neighbors. Due to this spatial isolation we can consider these states to be akin to “dangling bonds”. An example of this is shown in Fig. (6). This is a unique property of the amorphous systems as an ordered crystalline material will ensure that no atom is isolated in this manner. This observation further provides insight for mitigation of TLSs through increased order.

IV. MITIGATION STRATEGIES

Identification of low-frequency phonon modes as a source of TLSs in superconducting qubits provides an opportunity to determine mitigation strategies. Namely, we have established that these low-frequency phonon modes arise due to the amorphous nature of the system, allowing

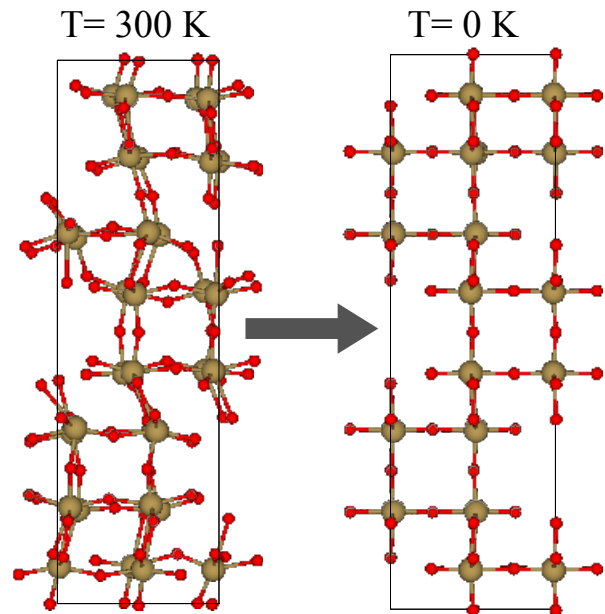


FIG. 7: (Left) Structure of amorphous Ta_2O_5 at room temperature after undergoing a melting/cooling cycle and being equilibrated. (Right) Upon relaxation of the structure at 0K the system returns to the crystalline, periodic structure in contrast to amorphous Al_2O_3 which lacks long-range order after relaxation at 0K.

for the existence of dangling bond-like structures within the bulk of the sample. One route to remove these defects is to work with a compound admitting increased order, such as a quasi-crystal, rather than an amorphous solid. With increased order isolated defects can be minimized.

It appears that amorphous oxides formed with heavier elements, such as TaO_x , are ideally positioned to reduce TLS density in modern superconducting qubits. The presence of heavier elements changes the energy landscape such that atomic configuration deviating from the convex hull can incur a greater energetic cost. It is expected that, when relaxed at zero temperature, amorphous TaO_x has a greater likelihood of returning to a crystalline or quasi-crystalline form. To investigate this claim we repeat the process utilized for generation of amorphous Al_2O_3 , applying it to a supercell of Ta_2O_5 containing 112 atoms. The same procedure is appropriate as the melting point of Ta_2O_5 is similar to that of Al_2O_3 at 2145K [34]. However, due to the increased mass of Ta versus Al, when the system is equilibrated, either in the liquid phase or at any other point, we choose to double the number of time steps for which the system is equilibrated. When equilibrating in the liquid phase, we also impose an ion temperature of 3000K to aid in vanquishing any remnant of the crystal structure.

Examining the final structures after equilibration at room temperature and zero temperature relaxation, shown in Fig. (7), it is striking that the systems ap-

pears to have returned to the ordered crystalline phase. This is in stark contrast to the amorphous Al_2O_3 structures which do not resemble the ordered solid counterpart. While this computation suggests increased order in samples of amorphous Ta_2O_5 relative to amorphous Al_2O_3 , future work is required to ensure this observation remains valid in the thermodynamic limit.

Despite the need for future work we remark that a separate study has examined the surfaces of amorphous TaO_x structures, revealing a decreased density of TLSs when compared to the lighter amorphous NbO_x [35]. This is in agreement with our observations that the density of surface dangling bonds may be reduced in heavier oxides. Evidence of this is provided in the appendix where the surface density of states for amorphous Al_2O_3 and amorphous Ta_2O_5 are compared.

V. DISCUSSION

In this work we have performed detailed first-principles computations to construct multiple samples of amorphous Al_2O_3 . Computing the phonon modes we identify low-frequency states exhibiting real-space localization and a dipole moment in agreement with that expected for TLSs in superconducting qubits which use amorphous Al_2O_3 as the Josephson junction barrier. We find that the low-frequency modes are inherent in amorphous Al_2O_3 due to the lack of order and can be mitigated by use of crystalline or quasi-crystalline materials for which such bulk defects are suppressed. The computationally available energies we probe are in sub THz range. We do believe that similar soft localized exci-

tations persist down to GHz range, relevant for device applications, and thus are viable candidates for TLS dephasers in SC qubits. This observation also applies to the existence of TLSs on the surfaces.

We also compare the amorphous amorphous Al_2O_3 with the Ta_2O_3 . We find that with similar protocol for sample preparation the Ta_2O_3 forms a regular crystalline structure and thus inherently is less disordered. We suggest that Ta_2O_3 as an optimal alternative.

Future work is required to establish the precise quasicrystalline structure of Ta_2O_3 as synthesized in current superconducting qubits for comparison with first-principles analysis. In addition further samples and larger system sizes are required to further limit any finite size effects.

ACKNOWLEDGMENTS

We are grateful to D. Pappas, Y. Rosen, J. Mutus and X. Wang for useful discussions. Work at NORDITA is supported by the Novo Nordisk Foundation and NordForsk. AB and JH were also supported by European Research Council under the European Union Seventh Framework ERS-2018-SYG 810451 HERO and by Knut and Alice Wallenberg Foundation Grant No. KAW 2019.0068. The computations were enabled by resources provided by the National Academic Infrastructure for Supercomputing in Sweden (NAISS), partially funded by the Swedish Research Council through grant agreement no. 2022-06725. This work is supported by the Novo Nordisk Foundation, Grant number NNF22SA0081175, NNF Quantum Computing Programme

-
- [1] Kjaergaard, M., Schwartz, M. E., Braumüller, J., Krantz, P., Wang, J. I.-J., Gustavsson, S., and Oliver, W. D., “Superconducting qubits: Current state of play,” *Annual Review of Condensed Matter Physics* **11**, 369–395 (2020).
- [2] Devoret, M. H., Wallraff, A., and Martinis, J. M., “Superconducting qubits: A short review,” *cond-mat/0411174* (2004).
- [3] Koch, J., Yu, T. M., Gambetta, J., Houck, A. A., Schuster, D. I., Majer, J., Blais, A., Devoret, M. H., Girvin, S. M., and Schoelkopf, R. J., “Charge-insensitive qubit design derived from the cooper pair box,” *Phys. Rev. A* **76**, 042319 (2007).
- [4] Krantz, P., Kjaergaard, M., Yan, F., Orlando, T. P., Gustavsson, S., and Oliver, W. D., “A quantum engineer’s guide to superconducting qubits,” *Applied physics reviews* **6** (2019), <https://doi.org/10.1063/1.5089550>.
- [5] Gordon, L., Abu-Farsakh, H., Janotti, A., and Van de Walle, C. G., “Hydrogen bonds in al_2o_3 as dissipative two-level systems in superconducting qubits,” *Sci. Rep.* **4**, 7590 (2014).
- [6] Bilmes, A., Zanker, S., Heimes, A., Marthaler, M., Schön, G., Weiss, G., Ustinov, A. V., and Lisenfeld, J., “Electronic decoherence of two-level systems in a josephson junction,” *Phys. Rev. B* **96**, 064504 (2017).
- [7] Müller, C., Shnirman, A., and Makhlin, Y., “Relaxation of josephson qubits due to strong coupling to two-level systems,” *Phys. Rev. B* **80**, 134517 (2009).
- [8] Ku, L.-C. and Yu, C. C., “Decoherence of a josephson qubit due to coupling to two-level systems,” *Phys. Rev. B* **72**, 024526 (2005).
- [9] James, D. F. V., Kwiat, P. G., Munro, W. J., and White, A. G., “Measurement of qubits,” *Phys. Rev. A* **64**, 052312 (2001).
- [10] Müller, C., Cole, J. H., and Lisenfeld, J., “Towards understanding two-level-systems in amorphous solids: insights from quantum circuits,” *Rep. Prog. Phys.* **82**, 124501 (2019).
- [11] Mansikkamäki, O., Tyner, A., Bilmes, A., Drozdov, I., and Balatsky, A., “Two-tone spectroscopy for the detection of two-level systems in superconducting qubits,” *arXiv:2404.14039* (2024), <https://doi.org/10.48550/arXiv.2404.14039>.
- [12] Crowley, K. D., McLellan, R. A., Dutta, A., Shumiya, N., Place, A. P. M., Le, X. H., Gang, Y., Madhavan, T., Bland, M. P., Chang, R., Khedkar, N., Feng, Y. C., Umbarkar, E. A., Gui, X., Rodgers, L. V. H., Jia, Y., Feld-

- man, M. M., Lyon, S. A., Liu, M., Cava, R. J., Houck, A. A., and de Leon, N. P., “Disentangling losses in tantalum superconducting circuits,” *Phys. Rev. X* **13**, 041005 (2023).
- [13] McRae, C. R. H., Wang, H., Gao, J., Vissers, M. R., Brecht, T., Dunsworth, A., Pappas, D. P., and Mutus, J., “Materials loss measurements using superconducting microwave resonators,” *Review of Scientific Instruments* **91**, 091101 (2020), https://pubs.aip.org/aip/rsi/article-pdf/doi/10.1063/5.0017378/19786221/091101_1_online.pdf.
- [14] Gunnarsson, D., Pirkkalainen, J.-M., Li, J., Paraoanu, G. S., Hakonen, P., Sillanpää, M., and Prunnila, M., “Dielectric losses in multi-layer josephson junction qubits,” *Superconductor Science and Technology* **26**, 085010 (2013).
- [15] Pritchard, P. G. and Rondinelli, J. M., “Suppressed paramagnetism in amorphous $\text{Ta}_{1-x}\text{Nb}_x\text{O}_5$ oxides and its link to superconducting qubit performance,” arXiv:2410.13160 (2024), <https://doi.org/10.48550/arXiv.2410.13160>.
- [16] Morrissey, K. J. and Carter, C. B., “Faceted grain boundaries in Al_2O_3 ,” *J. Am. Ceram. Soc.* **67**, 292–301 (1984).
- [17] Lee, S. K., Lee, S. B., Park, S. Y., Yi, Y. S., and Ahn, C. W., “Structure of amorphous aluminum oxide,” *Phys. Rev. Lett.* **103**, 095501 (2009).
- [18] Katiyar, P., Jin, C., and Narayan, R., “Electrical properties of amorphous aluminum oxide thin films,” *Acta Mater.* **53**, 2617–2622 (2005).
- [19] Cooper, N., Goringe, C., and McKenzie, D., “Density functional theory modelling of amorphous silicon,” *Comput. Mater. Sci.* **17**, 1–6 (2000).
- [20] McCulloch, D. G., McKenzie, D. R., and Goringe, C. M., “Ab initio simulations of the structure of amorphous carbon,” *Phys. Rev. B* **61**, 2349–2355 (2000).
- [21] Štich, I., Car, R., and Parrinello, M., “Amorphous silicon studied by ab initio molecular dynamics: Preparation, structure, and properties,” *Phys. Rev. B* **44**, 11092–11104 (1991).
- [22] Car, R. and Parrinello, M., “Structural, dynamical, and electronic properties of amorphous silicon: An ab initio molecular-dynamics study,” *Phys. Rev. Lett.* **60**, 204–207 (1988).
- [23] Car, R. and Parrinello, M., “Unified approach for molecular dynamics and density-functional theory,” *Phys. Rev. Lett.* **55**, 2471–2474 (1985).
- [24] Wesselinowa, J. M. and Kovachev, S., “Hardening and softening of soft phonon modes in ferroelectric thin films,” *Phys. Rev. B* **75**, 045411 (2007).
- [25] Giannozzi, P., Barone, O., Bonfà, P., Brunato, D., Car, R., Carnimeo, I., Cavazzoni, C., de Gironcoli, S., Delugas, P., Ferrari Ruffino, F., Ferretti, A., Marzari, N., Timrov, I., Urru, A., and Baroni, S., “Quantum espresso toward the exascale,” *J. Chem. Phys.* **152**, 154105 (2020).
- [26] Perdew, J. P., Burke, K., and Ernzerhof, M., “Generalized gradient approximation made simple,” *Phys. Rev. Lett.* **78**, 1396–1396 (1997).
- [27] Van Setten, M. J., Giantomassi, M., Bousquet, E., Verstraete, M. J., Hamann, D. R., Gonze, X., and Rignanese, G.-M., “The pseudodojo: Training and grading a 85 element optimized norm-conserving pseudopotential table,” *Comput. Phys. Commun.* **226**, 39–54 (2018).
- [28] Schneider, S. J. and McDaniel, C., “Effect of environment upon the melting point of Al_2O_3 ,” *Journal of Research of the National Bureau of Standards. Section A, Physics and Chemistry* **71**, 317 (1967).
- [29] Chen, C. and Ong, S. P., “A universal graph deep learning interatomic potential for the periodic table,” *Nature Computational Science* **2**, 718–728 (2022).
- [30] Deng, B., Zhong, P., Jun, K., Riebesell, J., Han, K., Bartel, C. J., and Ceder, G., “Chgnet as a pretrained universal neural network potential for charge-informed atomistic modelling,” *Nature Machine Intelligence* **5**, 1031–1041 (2023).
- [31] Batatia, I., Kovacs, D. P., Simm, G., Ortner, C., and Csányi, G., “Mace: Higher order equivariant message passing neural networks for fast and accurate force fields,” *Advances in Neural Information Processing Systems* **35**, 11423–11436 (2022).
- [32] Lisenfeld, J., Grabovskij, G. J., Müller, C., Cole, J. H., Weiss, G., and Ustinov, A. V., “Observation of directly interacting coherent two-level systems in an amorphous material,” *Nat. Commun.* **6**, 6182 (2015).
- [33] Hung, C.-C., Yu, L., Foroozani, N., Fritz, S., Gerthsen, D., and Osborn, K. D., “Probing hundreds of individual quantum defects in polycrystalline and amorphous alumina,” *Phys. Rev. Appl.* **17**, 034025 (2022).
- [34] Stewart, D. A., “Diffusion of oxygen in amorphous tantalum oxide,” *Phys. Rev. Mater.* **3**, 055605 (2019).
- [35] Wang, Z., Yu, C. C., and Wu, R., “Why superconducting ta qubits have fewer tunneling two-level systems at the air-oxide interface than nb qubits,” arXiv:2405.09842 (2024).
- [36] Pizzi, G., Vitale, V., Arita, R., Blugel, S., Freimuth, F., Géranton, G., Gibertini, M., Gresch, D., Johnson, C., Koretsune, T., Ibañez-Azpiroz, J., Lee, H., Lihm, J.-M., Marchand, D., Marrazzo, A., Mokrousov, Y., Mustafa, J. I., Nohara, Y., Nomura, Y., Paulatto, L., Poncé, S., Ponweiser, T., Qiao, J., Thole, F., Tsirkin, S. S., Wierzbowska, M., Marzari, N., Vanderbilt, D., Souza, I., Mostofi, A. A., and Yates, J. R., “Wannier90 as a community code: new features and applications,” *J. Phys. Condens. Matter* **32**, 165902 (2020).

Appendix A: Analysis of electronic density of states

In the main body we focus primarily on the identification of soft modes in the phonon spectra as potential two-level systems (TLSs), hastening decoherence in modern superconducting qubits. Computation of the phonon modes was done for bulk samples of amorphous Al_2O_3 (amorphous Al_2O_3). This is necessary due to the immense computational expense associated with the generation of large amorphous Al_2O_3 samples within first-principles, and subsequent computation of the phonon modes. Despite computational considerations limiting analysis of phonon soft modes to the bulk, it is important to consider the surfaces of amorphous Al_2O_3 . Surfaces can support a high-density of dangling bonds manifesting as surface roughness.

Following the observations of dangling bonds in the bulk explored in the main body, dangling bonds on the surface of amorphous Al_2O_3 are likely candidates for soft phonon modes, i.e. TLSs. Additionally, dangling bonds on the surface can support low-energy electronic bound

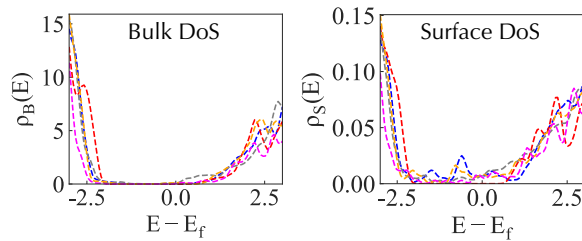


FIG. 8: (left) Bulk density of states for five distinct samples of amorphous Al_2O_3 . Each displays a robust gap in the electronic spectra at the Fermi level. (right) Density of states for five distinct samples of amorphous Al_2O_3 upon applying open boundary conditions along both the x and y directions, revealing emergent, surface bound electronic states within the mid-gap.

states. As such, probing the electronic density of states on the surface can be used to determine surface roughness and the density of TLSs. In order to model the surface of amorphous Al_2O_3 and compute the density of states, we construct real-space tight-binding models for each of the amorphous Al_2O_3 samples generated in the main body using the Wannier90 software package[36]. The bulk electronic states of the tight-binding model precisely matches that computed from first-principles in each case and is shown for the five amorphous samples in Fig. (9). In each

case we note the presence of a clean, insulating band-gap in line with expectations from experimental studies.

Utilizing the tight-binding models, we then consider the electronic density of states upon imposing open boundary conditions along the x and y directions and recompute the electronic density of states. The results shown in the left panel of Fig. (8) detail the emergence of low-energy mid-gap electronic state, which must be localized on the surface when comparing to the results shown in the right panel of Fig. (8). To investigate this further, we compute the spatially resolved local density of states at zero energy with the results shown in Fig. (9). These figures demonstrate that the resulting low-energy electronic states on the surface are localized, not extended, in correspondence with the presence of surface roughness and dangling bonds.

For completeness, we compare the low-energy electronic density of states on the surface with that computed for amorphous Ta_2O_5 . The bulk electronic density of states for two samples of amorphous Ta_2O_5 are shown in Fig. (10) along with the electronic density of states upon imposing open boundary conditions along the x and y directions. In agreement with the observation that amorphous Ta_2O_5 supports a more ordered structure, reducing surface roughness and the density of TLSs, the magnitude of mid-gap electronic density of states is reduced compared with amorphous Al_2O_3 . This is in alignment with the conclusions reached in Ref. [35], that the surface of amorphous Ta_2O_5 will support a reduced density of TLSs.

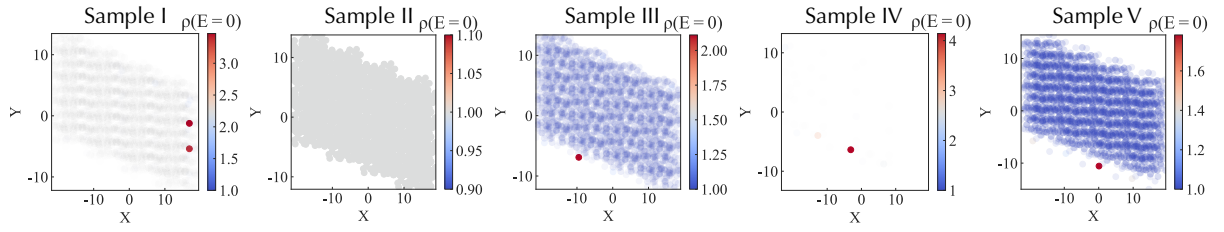


FIG. 9: Spatially resolved local density of states at the Fermi level for five distinct samples of amorphous Al_2O_3 upon application of open-boundary conditions along the x and y directions. Red points mark locations of greatest spectral density, they are located on the sample and spatially isolated in each case, revealing that the low-energy density of states seen in the right panel of Fig. (8) are localized surface modes.

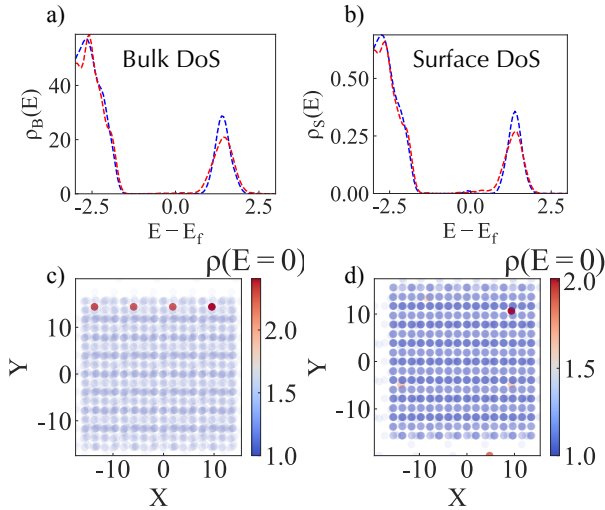


FIG. 10: (a) Bulk density of states for two distinct samples of amorphous Ta_2O_5 . Each displays a robust gap in the electronic spectra at the Fermi level. (b) Density of states for the same samples of amorphous Ta_2O_5 when applying open boundary conditions along both the x and y directions. While the gap is softened, the density of surface bound mid-gap electronic states is reduced compared to amorphous Al_2O_3 . (c)-(d) The spatially resolved density of states at the Fermi energy in the x - y plane for the two samples of amorphous Ta_2O_5 , demonstrating that any mid-gap states remain surface bound.